SUPPORTING INFORMATION

It is Supporting Information data for the publication 'An insight into separating H_2 from natural gas/H_2 mixtures using Mg-based systems'

Mateusz Balcerzak,*[a,b,c] Robert Urbanczyk,[a,d] Fabian Lange,[a] Francis Anne Helm,[a] Jan Ternieden[a] and Michael Felderhoff[a]

[a] Heterogeneous Catalysis Department, Max-Planck-Institut für Kohlenforschung, Kaiser-Wilhelm Platz, 45470, Mülheim an der Ruhr, Germany

[b] Hydrogen and Fuel Cell Center (ZBT), Carl-Benz-Straße 201, 47057 Duisburg, Germany

[c] Institute of Materials Science and Engineering, Poznan University of Technology, Poznan 61-138, Poland

[d] F4 Gasprozesstechnik & Energieverfahrenstechnik, Institut für Umwelt & Energie, Technik & Analytik e. V., Bliersheimer Str. 58 – 60, 47229 Duisburg, Germany

* E-mail: balcerzak@kofo.mpg.de

The SI was created to not only present but also discuss some of the supplementary research data. The data and descriptions were divided into ten subchapters.

Table of Contents

S1. Transition of energy economy in Germany

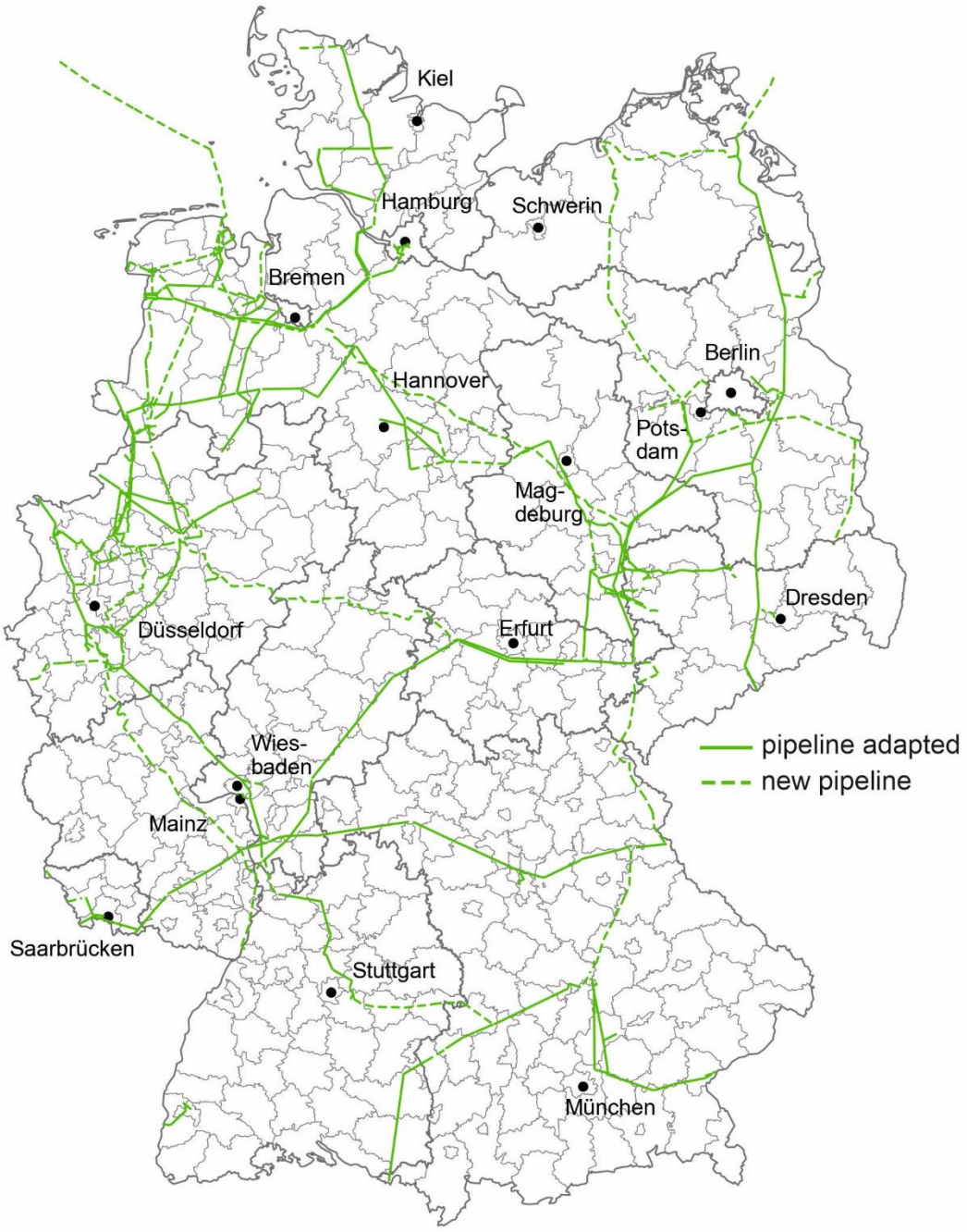

Fig. S1 Development of the hydrogen core network in Germany. Picture adapted from [S1]

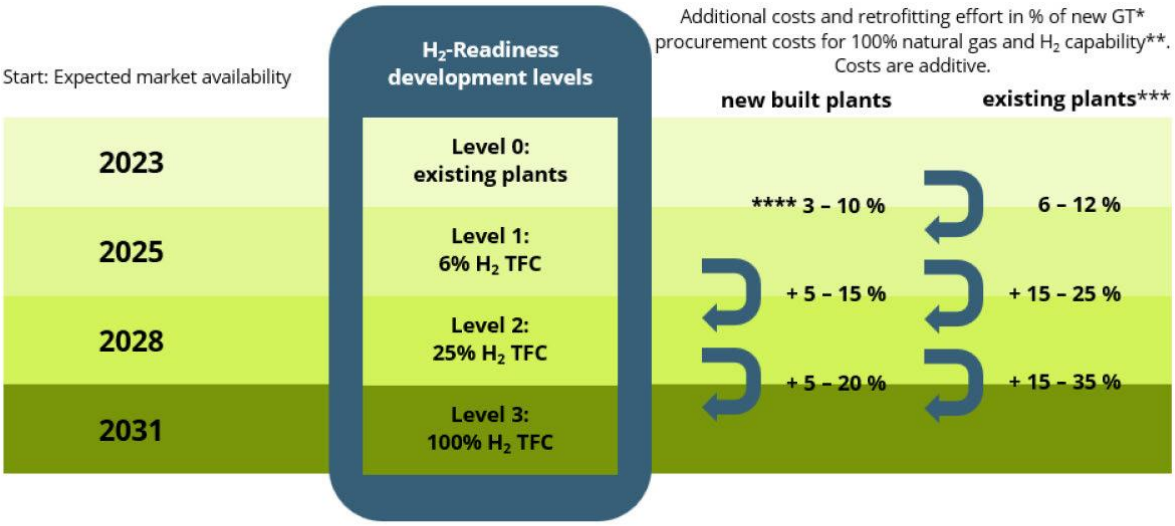

* The scope of retrofitting refers to the retrofitting of all components necessary for operation, but the cost reference is the gas turbine as core component

** A pre-planned modular design of the ancillary systems can significantly reduce retrofitting costs for new plants (H_2 capability)

*** In many cases, retrofitting existing systems can make much more economic sense, even if measures to extend the service life, etc. still have to be carried out on the GTP

**** Additional costs for H_2 capability

Fig. S2. Development levels of H_2 readiness for gas turbine plants [S2].

For many years, applications such as gas turbines or burners in the glass industry have operated on a foundation of relatively stable gas quality. However, because of changing heating values and other specifications (Wobbe index or flame velocity) of primary H_2 and CH_4 in the gas mixture, the above-mentioned applications must be adjusted to the new conditions. For instance, gas turbine plants are planned to achieve Level 1 of readiness for H_2-contributed gas mixture in 2025 (Fig. S2) [S2].

Level 1 means that the thermal firing capacity (TFC) equals 6%, corresponding to a volume fraction of H_2 in the gas mixture of approximately 16%. Level 2 with 25% of TFC means approx. 52% of H_2 in the gas mixture in 2028. Level 3 of TFC, equal to 100%, will be achieved in 2031 and stands for pure H_2. Therefore, regarding the mentioned example of gas turbines, which will work with different fuel blends with H_2, until the hydrogen economy is completely implemented, there will be a time when intermediate technologies like Hydrogen separation techniques must be applied to fulfil the economy transition goals.

S2. Materials and gases

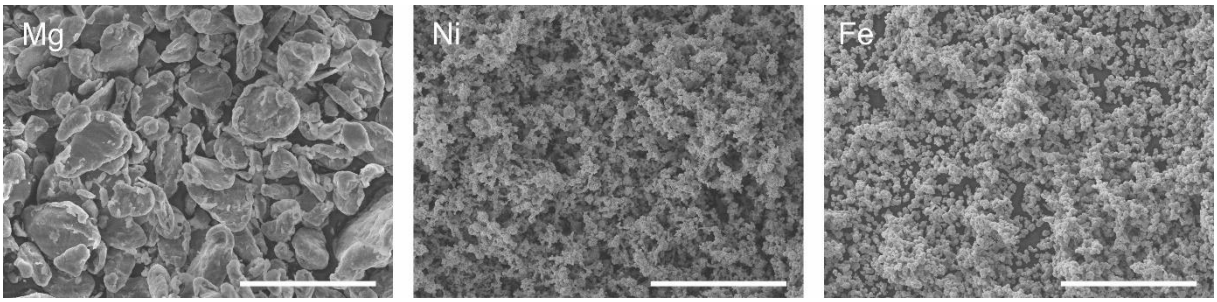

Fig. S3 SE-SEM images obtained for Mg, Ni and Fe powders. Scale bars: 100 µm.

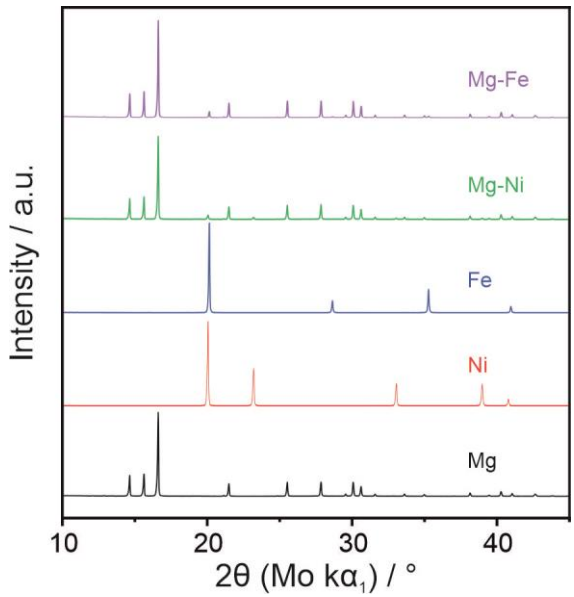

Fig. S4 XRD patterns obtained for pure elements (Mg, Ni, and Fe) and Mg-Ni, Mg-Fe systems after one hour of shaking.

Table S1 Composition of natural gas (Air Liquide, Natural gas L) provided by the supplier and as analyzed by GC (using 30m, RT-Q-Bond 0.53/20df G/785 column and 0.5 bar He)

	CH_4 / %	C_2H_6 / %	N_2 / %	CO_2 / %	C_3H_8 / %	C_4H_{10} / %
Air Liquide specification	83 – 99	<12	0.5 - 3	<1.5	0.1 - 1	0.1 - 1
GC	92.50	-	7.47	0.03	-	-

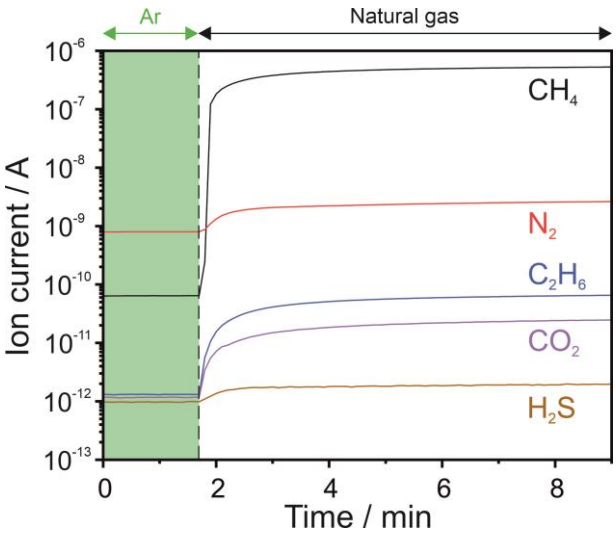

Fig. S5 Results of mass spectroscopy performed on natural gas (Air Liquide, Natural gas L). Initially, the apparatus was fed with Ar flowing through the system (to determine the background signal level). The vertical line points to the moment when Ar was exchanged for natural gas.

The composition of the natural gas was evaluated by gas chromatography (GC) and mass spectroscopy (MS; in this case, only qualitatively) and compared with the supplier specification (Fig. S5, Table S1). The GC results indicate that the CH_4 and N_2 concentrations exceed 92 % and 7 %, respectively. The gas composition included traces of C_2H_6, CO_2, and H_2S. The experimental analysis did not reveal the presence of C_3H_8 or C_4H_{10} (n) – which were stated by the supplier. The GC and MS data showed that the actual composition of natural gas differs slightly from the supplier specification.

S3. Calibration of gas chromatography

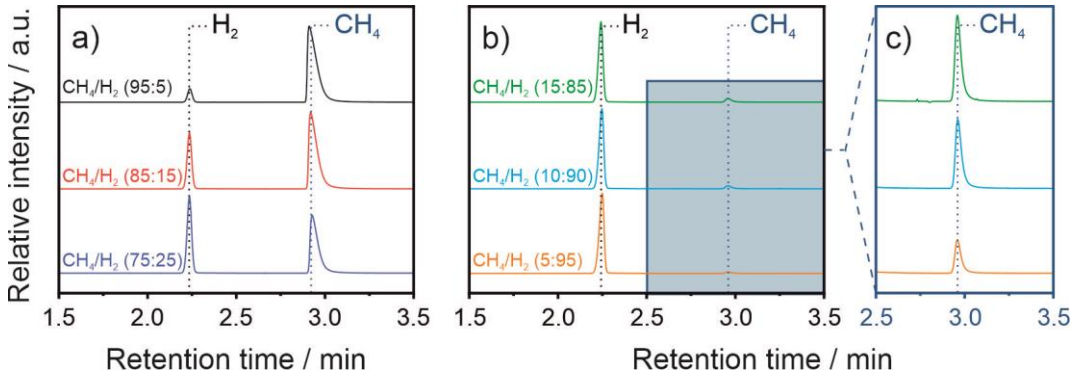

Fig. S6 Results of GC made on CH_4/H_2 gas mixtures with different concentrations of CH_4 and H_2: (a) relatively low H_2 concentrations; (b,c) relatively high H_2 concentrations. The dark blue area in (b) points out the region of patterns enlarged in (c). The percentage concentrations of each gas component are shown in the brackets. The dotted lines indicate the position of H_2 and CH_4 peaks.

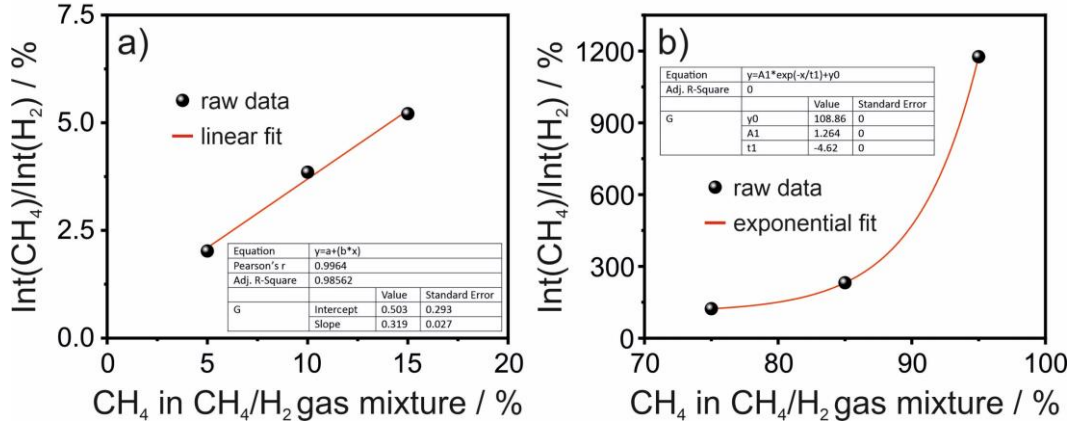

Fig. S7 Calibration curves for GC analyses of the CH_4 content in the CH_4/H_2 gas mixtures: (a) low CH_4 concentrations; (b) high CH_4 concentrations. Int in the y-axis description stands for Integral.

The calibration curves (Fig. S7) are based on the GC results (Fig. S6) obtained for the standard gas mixture concentrations (prepared on-site using the calibrated EL-FLOW Bronkhorst mass flow meters). The curve of the relatively low CH_4 concentration in the CH_4/H_2 gas mixture (Fig. S7a) enables the quantitative determination of the H_2 concentration/purity in the gas mixture desorbed from the metal hydride. The curve of the relatively high CH_4 concentration in the CH_4/H_2 gas mixture (Fig. S7b) was used to evaluate the prepared on-site gas mixtures (5L bottles of gas mixtures).

S4. The gas-separation setup

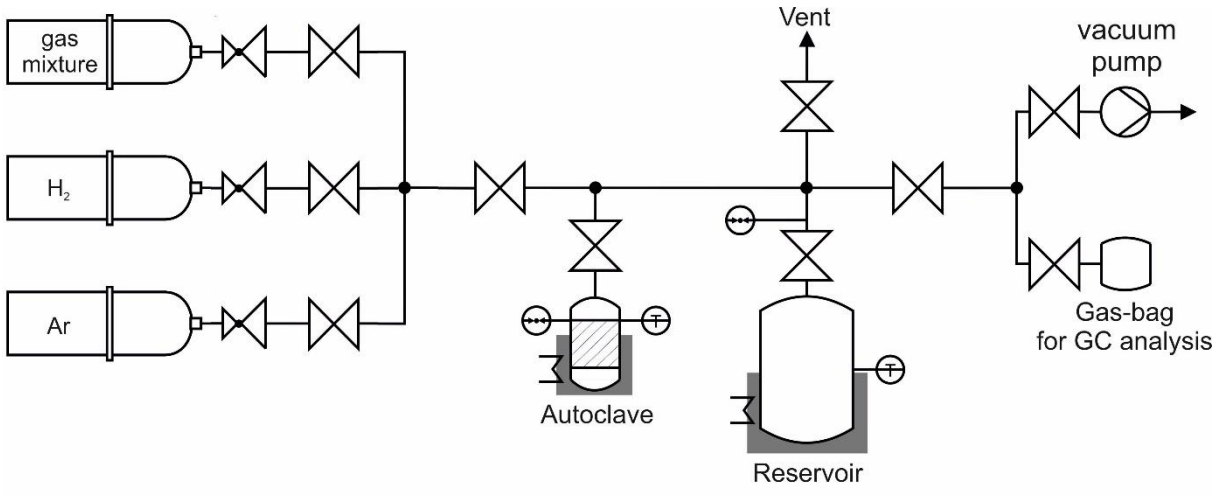

Fig. S8 Scheme of the gas-separation setup

The setup scheme for conducting experiments on the separation of hydrogen from gas mixtures is shown in Fig. S8. The main part of the setup is the autoclave, which is located in the central position of the sketch. In the autoclave, the gas separation reaction has taken place, thus both hydrogenation of Mg and subsequent dehydrogenation of the MgH_2 (and other minor phases). The autoclave was manufactured on-site as a batch reactor with an inner volume of 100 mL. The material used to fabricate the autoclave was austenitic steel according to the DIN EN 10881-1 standard, numbered X6NiCrTiMoVB25-15-2 (other denominations: W.-Nr. 1.4980, Alloy A-286). The autoclave could be opened/closed from one side via a flange/lid system with six screws and was sealed with a gold O-ring gasket. The autoclave filled with Mg-based system was half-inserted into an electrically heated furnace during the experiments. The upper part of the autoclave was only thermally insulated. In this way, the heater actively influenced the lower part of the autoclave containing the active material, while the upper part of the autoclave was at a lower temperature (especially in the area of the flange/lid system), which prevented leaks during the operation of the autoclave. The pressure inside the autoclave was measured using a JUMO dTrans p30 pressure transmitter. The temperature of the active material was controlled using a K-type thermocouple.

The calculation of the gravimetric hydrogen storage capacity (of formed hydride) during the H_2 separation was accomplished by measuring both the pressure increase and the temperature of H_2 in the reservoir (which was connected to the autoclave) during the dehydrogenation process. The reservoir's internal volume was 500 mL. It had a heating system, which maintained the gas temperature in the reservoir at a constant 30°C. The pressure transducer for measuring the gas pressure in the reservoir was type PAA- 33X provided by KELLER Gesellschaft für Druckmesstechnik GmbH, and a type K thermocouple controlled the temperature. Pressure and temperature values in the autoclave and reservoir were recorded by the JUMO 2000. Appropriate temperature controller and temperature limiter systems supervised both heaters.

As shown in Fig. S8, the main parts of the setup (autoclave and reservoir) were connected via valves and pressure reducers to three gas cylinders containing H_2, Ar, and a gas mixture.

H_2 was used to activate the Mg-based systems placed inside the autoclave, as well as for hydrogenation tests with pure H_2. The activation protocol has already been published elsewhere [S3]. Ar was used to purge the sample from the residual gas after separation of H_2 - from the remaining gas mixture present in the autoclave after subsequent cooling. In addition to the Ar purge, a short evacuation (under dynamic vacuum) of the hydrogenated Mg-based systems was also applied to get rid of any gases that were still in the reactor. The abovementioned purging/evacuation allowed us to investigate the quality of released H_2 in in the subsequent dehydrogenation process (using GC). After the dehydrogenation process was completed, the desorbed gas was expanded through a valve connected to the GC gas sampling bag (shown on the right side in Fig S8). The vent system was used to release the overpressure after the hydrogenation and dehydrogenation process as well as during the flushing of the system with Ar.

S5. Hydrogen absorption and desorption in Mg-Ni system

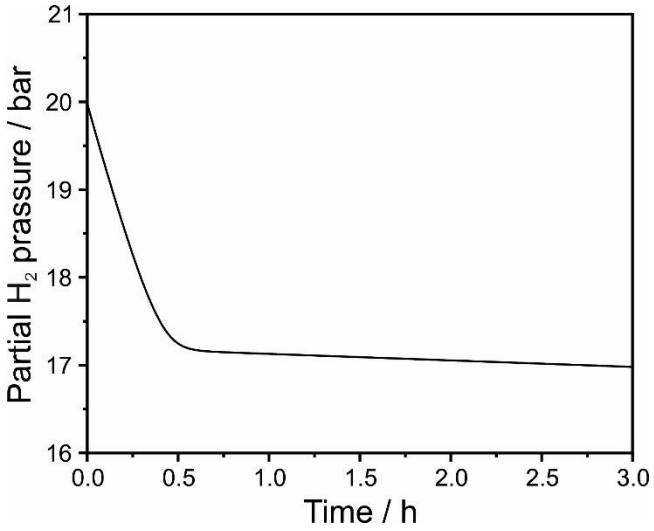

Fig. S9 Change of the partial H_2 pressure in time (representing H_2 absorption) in autoclave loaded with Mg-Ni system during hydrogenation with 100 bar of CH_4/H_2 gas mixture (20 bar of partial H_2 pressure) at 350 °C.

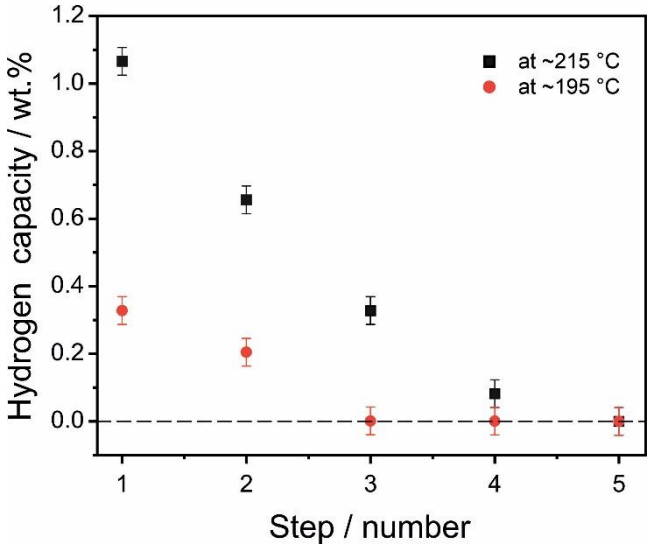

Fig. S10 Amount of H_2 desorbed from hydrogenated Mg-Ni system in the following steps of dehydrogenation at ~195 °C and ~ 215 °C. Each dehydrogenation step lasted five minutes. Prior to first step and between each subsequent one, the autoclave filled with hydrogenated Mg-Ni system was evacuated under vacuum for 10 seconds.

The hydrogenated Mg-Ni system was used to estimate the amount of H_2 desorbed from the material at ~195 °C and ~ 215 °C. The material after hydrogenation was evacuated under vacuum for 10 seconds and then left for five minutes to determine amount of desorbed H_2. The amount of desorbed hydrogen is presented in Fig. S10 (step 1 at each temperature). The process of evacuation (10 seconds) and dehydrogenation (five minutes) was repeated stepwise using the same material.

Fig. S10 shows that Mg-Ni system desorbs more than 1 wt.% H_2 within the first dehydrogenation step at ~ 215 °C. The folowing dehydrogenation steps performed at ~ 215 °C

show reduction of desorbed H_2 in the following dehydrogenation steps, to reach no dehydrogenation in the fifth step. The amount of dehydrogenated H_2 is significantly lower when the process is performed at ~195 °C. Not more than 0.4 wt.% H_2 is desorbed in the first step at this temperature. Moreover, the material does not desorb any hydrogen already in the third step at ~195 °C.

The data presented in Fig. S10 are particularly useful when one considers that both systems (Mg-Ni and Mg-Fe), were vented, and the used setup was five times purged using an alternately dynamic vacuum and 5 bar Ar, between each hydrogenation and dehydrogenation (in H_2 separation experiments presented in Fig. 1 a,b). This venting and purging process corresponds to the part of the H_2 desorbed in the first step of dehydrogenation presented in Fig. S10.

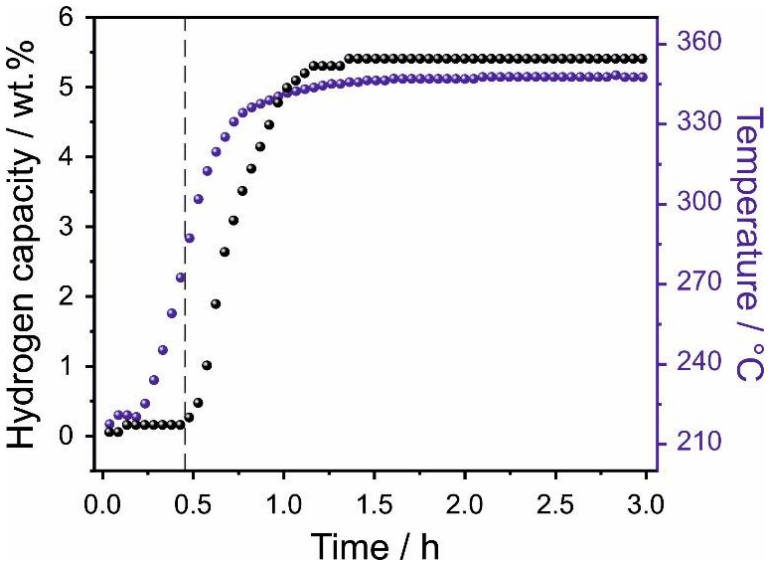

Fig. S11 H_2 desorption kinetic curve recorded for the hydrogenated Mg-Ni system during its heating from ~215 °C to ~350 °C. The dashed line indicates the start of dynamic H_2 desorption.

S6. Mg-Ni system after separation of H_2 from CH_4/H_2 and NG/H_2 gas mixtures

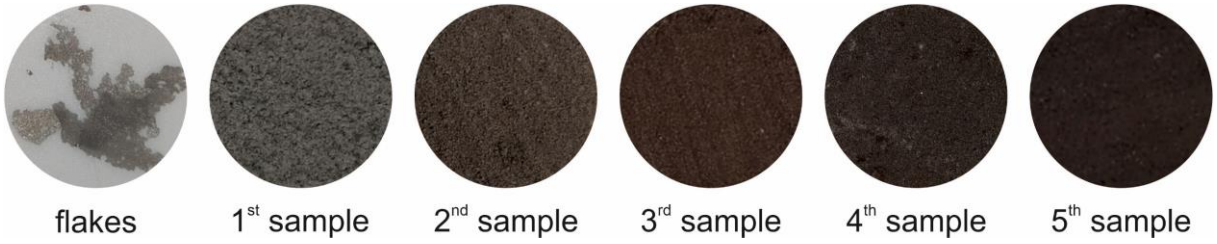

Fig. S12 Pictures of the flakes and powders of the Mg-Ni system material after cycles of hydrogenation/dehydrogenation experiments under 20 bar H_2, 100 bar of CH_4/H_2 gas mixture (20 bar of partial H_2 pressure), and 100 bar of natural gas/H_2 gas mixture (20 bar of partial H_2 pressure). The sample/layer numbers correspond to the number presented in Fig. 2a.

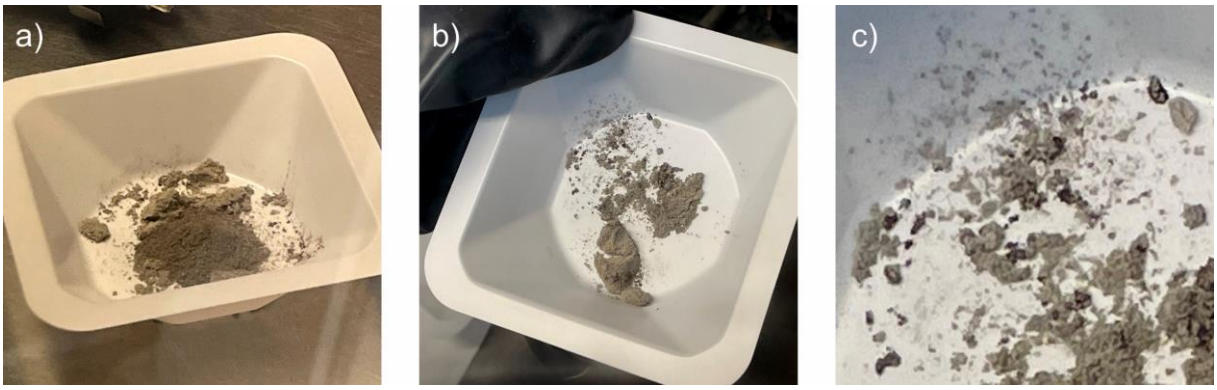

Fig. S13 (a,b,c) Photos of the Mg-Ni system material collected from the autoclave after a series of hydrogenation/dehydrogenation experiments run under 20 bar H_2, 100 bar of CH_4/H_2 gas mixture (20 bar of partial H_2 pressure), and 100 bar of natural gas/H_2 gas mixture (20 bar of partial H_2 pressure). When taking photos, the samples were placed in a glove box filled with Ar.

Fig. S13 presents a distinction between different parts of the Mg-Ni system after the gas separation experiments. The bright granules and darker powder, presented in Fig. S13a, correspond to the 1st and 2nd layers' samples (presented graphically in Fig. 2a), respectively. Fig S13b,c presents the difference in colour between MgH_2 light grey granules (a major part of the granules) and dark red/brown spots of Mg_2NiH_4 (present mostly on the surface of the granules).

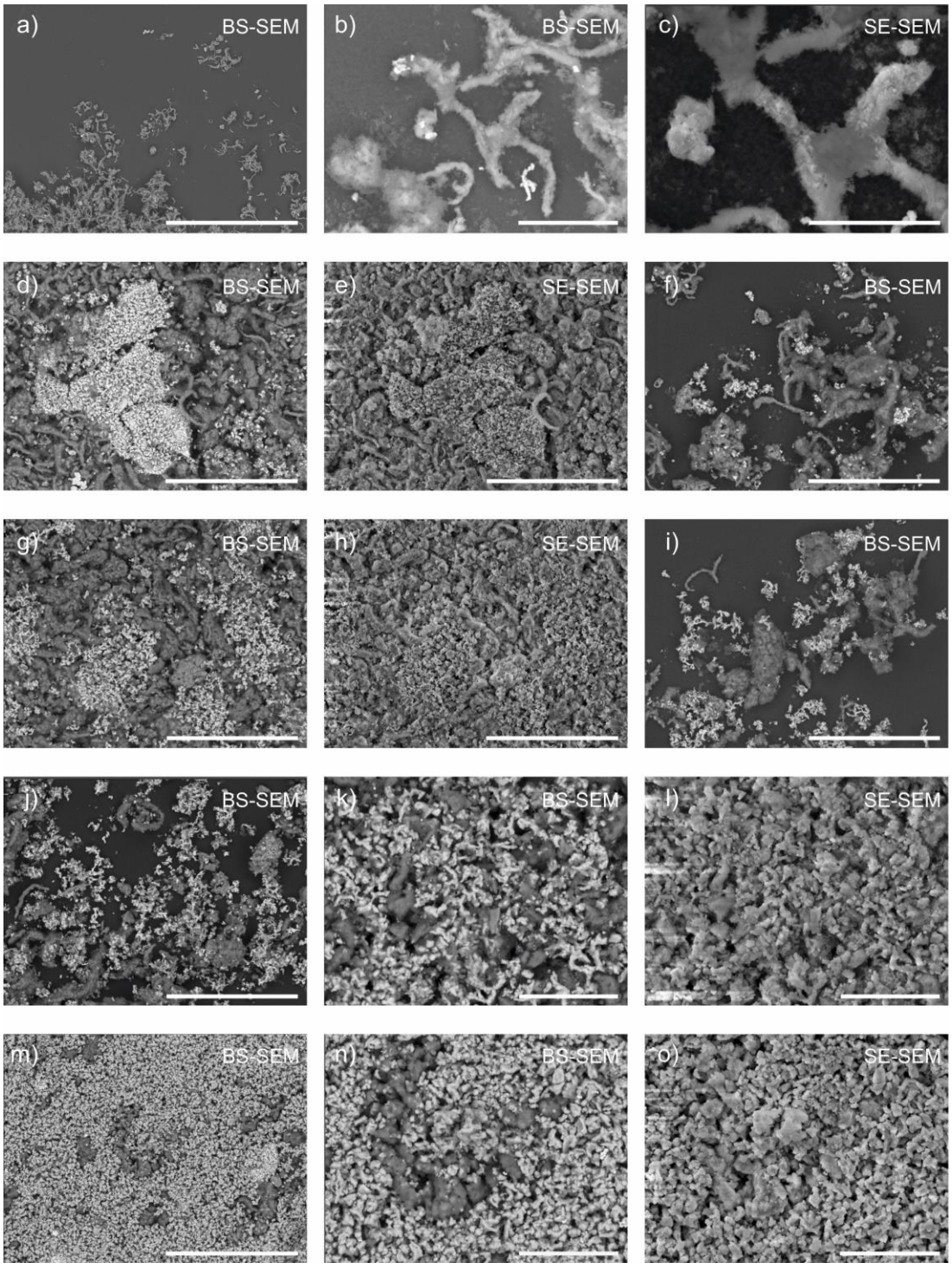

Fig. S14 SE-SEM and BS-SEM images obtained at different magnifications for the samples collected from the Mg-Ni system after cyclic separation experiments (15 kV): 1st (a,b,c), 2nd (d,e,f,), 3rd (g,h,i), 4th (j,k,l), 5th (m,n,o). The layers' sample numbers correspond to the number presented in Fig. 2a. Scale bars: 500 µm (a), 100 µm (d,e,f,g,h,l,j,m), 30 µm (b,k,l,n,o), 20 µm (c).

Fig. S14 shows the morphology of samples collected from different layers of the Mg-Ni system after separation experiments. The darker (less dense) part of the material is mostly composed of MgH_2 while the brighter (denser) part of the Ni-containing phases.

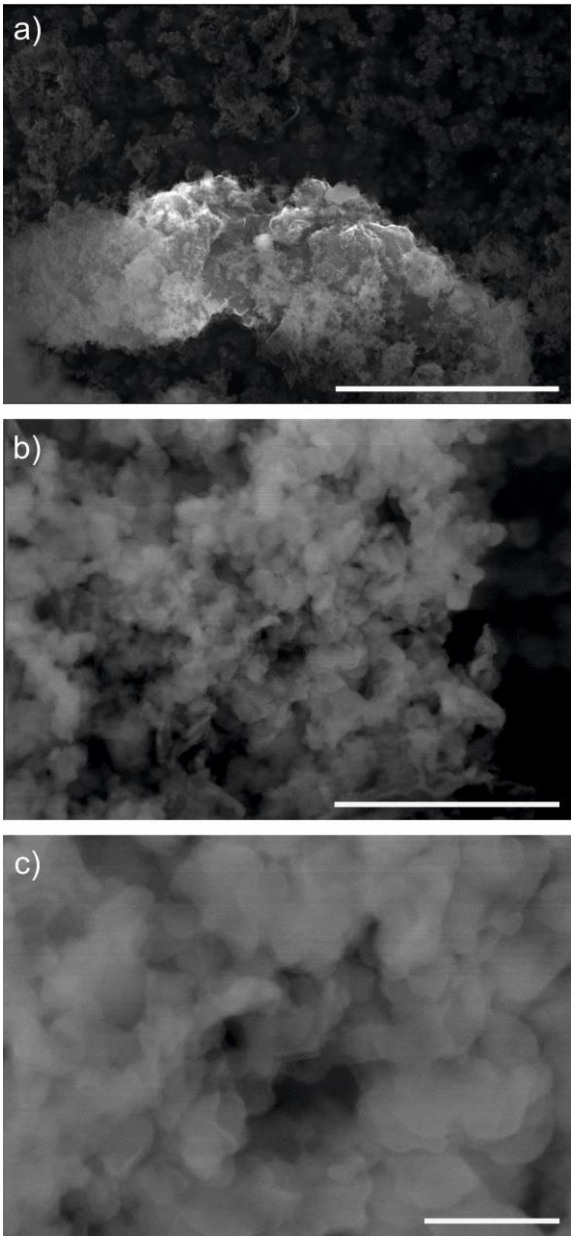

Fig. S15 SE-SEM images obtained at different magnifications for the 1st layer' sample collected from the Mg-Ni system after cyclic separation experiments (30 kV). The sample number corresponds to the number presented in Fig. 2a. Scale bars: 5 µm (a), 500 nm (b), 100 nm (c).

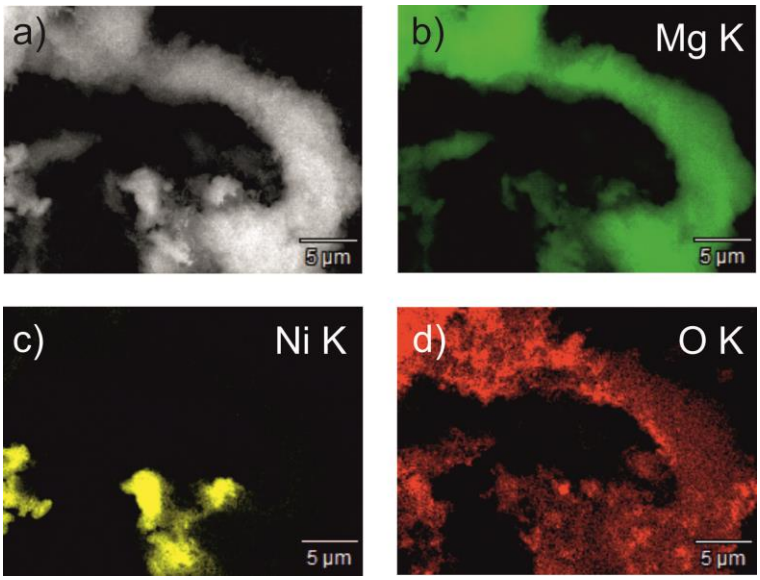

Fig. S16 SE-SEM (a) and corresponding EDX images (b,c,d) of the 1st layer' sample collected from the Mg-Ni system after cyclic separation experiments (30 kV). The sample number correspond to the number presented in Fig. 2a.

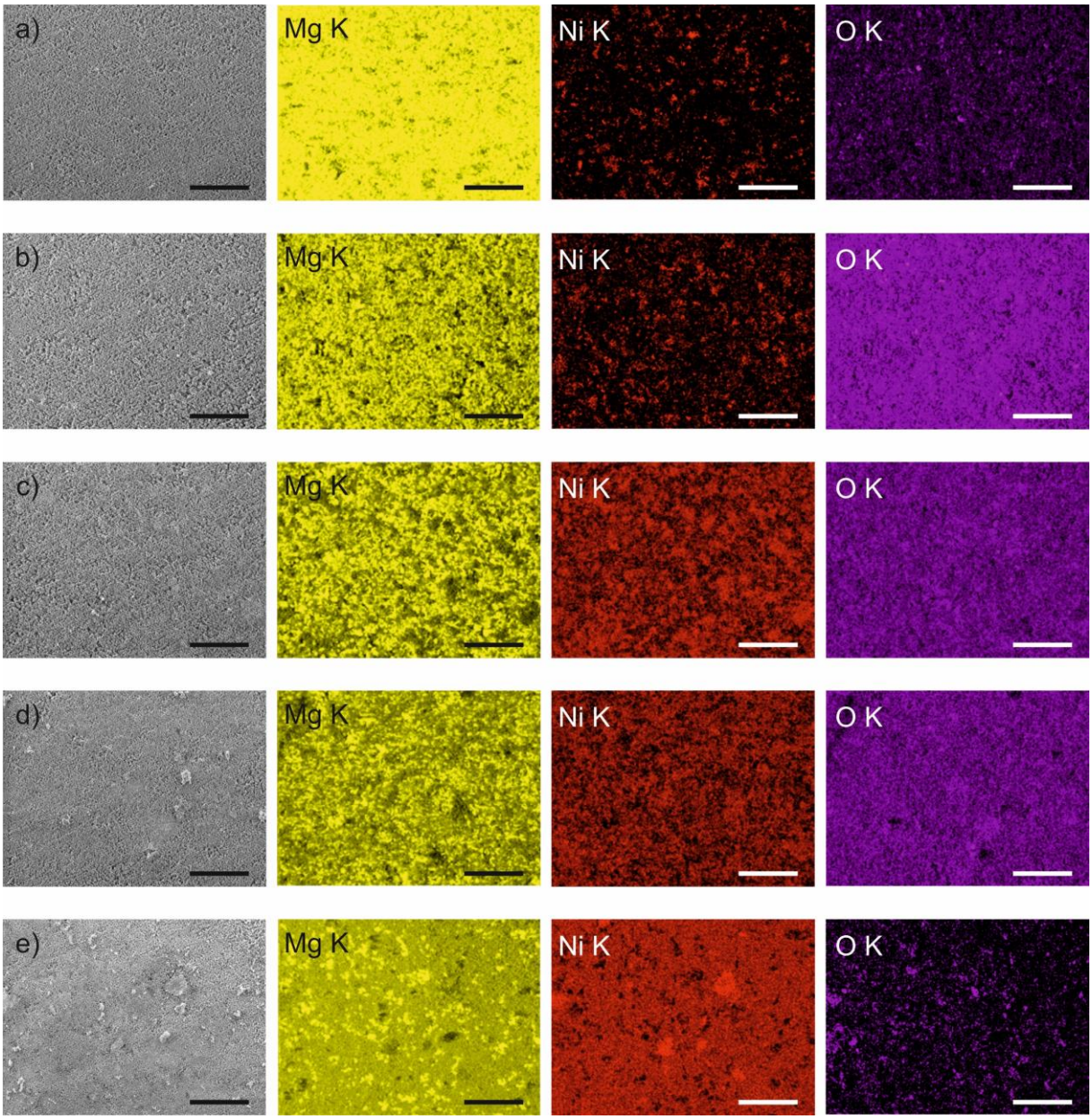

Fig. S17 SE-SEM micrographs and corresponding EDX images of the samples collected from different layers of the Mg-Ni system after cyclic separation experiments (15 kV): 1st (a), 2nd (b), 3rd (c), 4th (d), 5th (e). The sample numbers correspond to the number presented in Fig. 2a. Scale bars in all cases: 250 µm

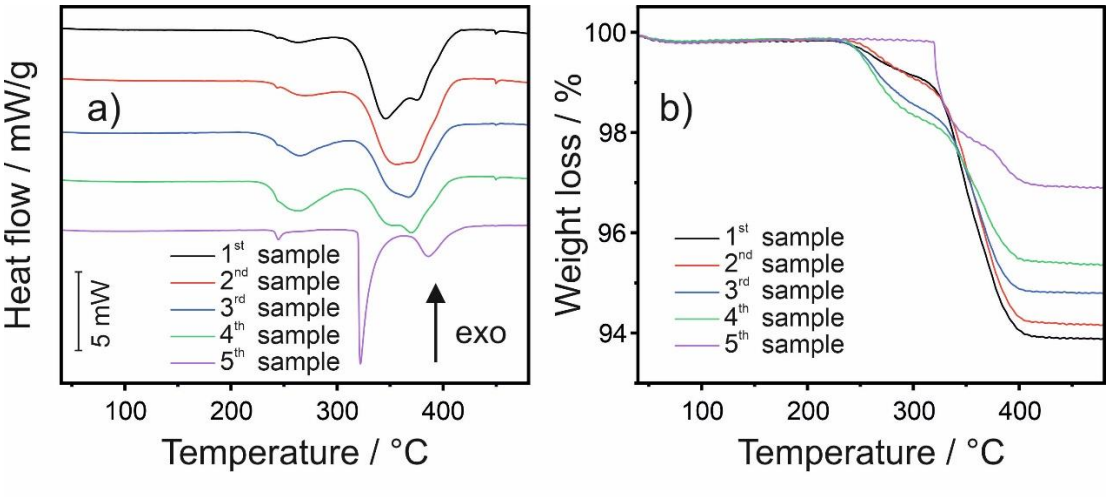

Fig. S18 DSC (a) and TG (b) curves obtained for the hydrogenated Mg-Ni system powder samples collected from different layers (the sample numbers correspond to the number presented in Fig. 2a) in the autoclave after a series of hydrogenation/dehydrogenation experiments run under 20 bar H_2, 100 bar of CH_4/H_2 gas mixture (20 bar of partial H_2 pressure), and 100 bar of natural gas/H_2 gas mixture (20 bar of partial H_2 pressure). The heating was performed at 10 °C/min. The heat flow has been normalized to the mass of the sample.

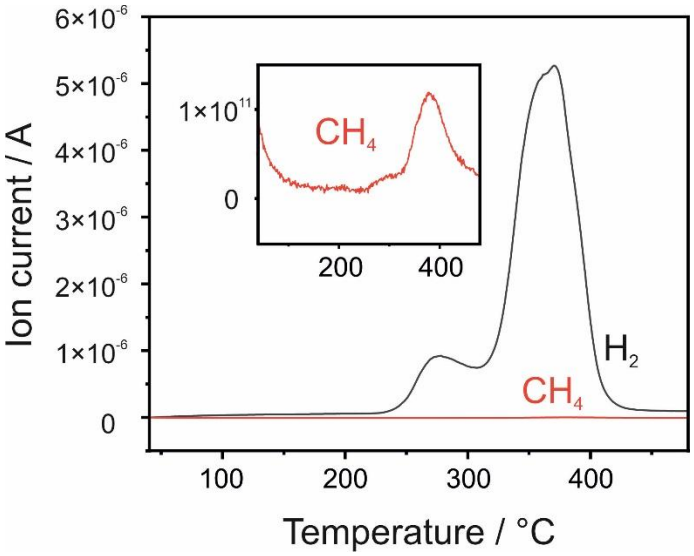

Fig. S19 Results of MS performed on the gases desorbed during TG/DSC experiment (10 °C/min) of hydrogenated Mg-Ni system (2nd layer' sample presented in Fig. 2a). The MS was connected directly to the outlet line of TG/DSC device.

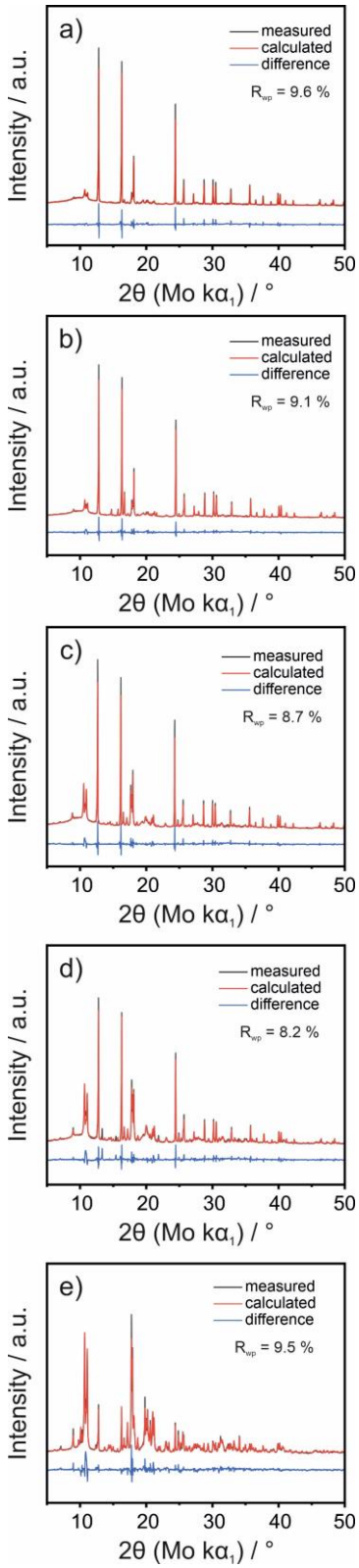

Fig. S20 XRD patterns and Rietveld refinement plots of the samples collected from different layers of the Mg-Ni system after cyclic separation experiments: 1st (a), 2nd (b), 3rd (c), 4th (d), 5th (e). The patterns were fitted using the following phases: Mg ICSD-258531 (ICSD release 2024.1), $Mg_2NiH_{0.29}$ ICSD-49534 (ICSD release 2024.1), Mg_2NiH_4 - monoclinic ICSD-201606 (ICSD release 2024.1), Mg_2NiH_4 cubic ICSD-600065 (ICSD release 2024.1), MgH_2 ICSD-155807 (ICSD release 2024.1), $MgNi_2$ ICSD-193568 (ICSD release 2024.1), MgO ICSD-158103 (ICSD release 2024.1), Ni ICSD-8688 (ICSD release 2024.1). The sample numbers correspond to the number presented in Fig. 2a.

S7. Mg-Fe system after separation of H_2 from CH_4/H_2 and NG/H_2 gas mixtures

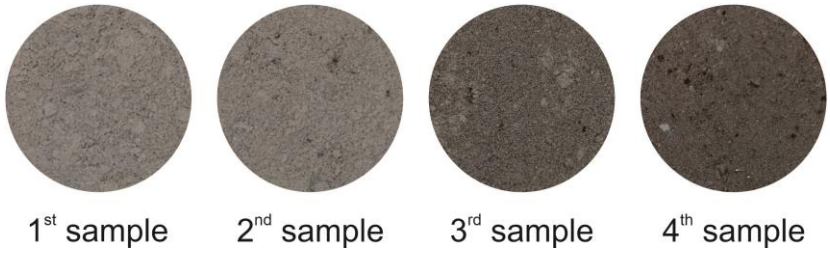

Fig. S21 Pictures of the powders of the Mg-Fe system material after cycles of hydrogenation/dehydrogenation experiments under 20 bar H_2, 100 bar of CH_4/H_2 gas mixture (20 bar of partial H_2 pressure), and 100 bar of natural gas/H_2 gas mixture (20 bar of partial H_2 pressure). The sample/layer numbers correspond to the number presented in Fig. 4a.

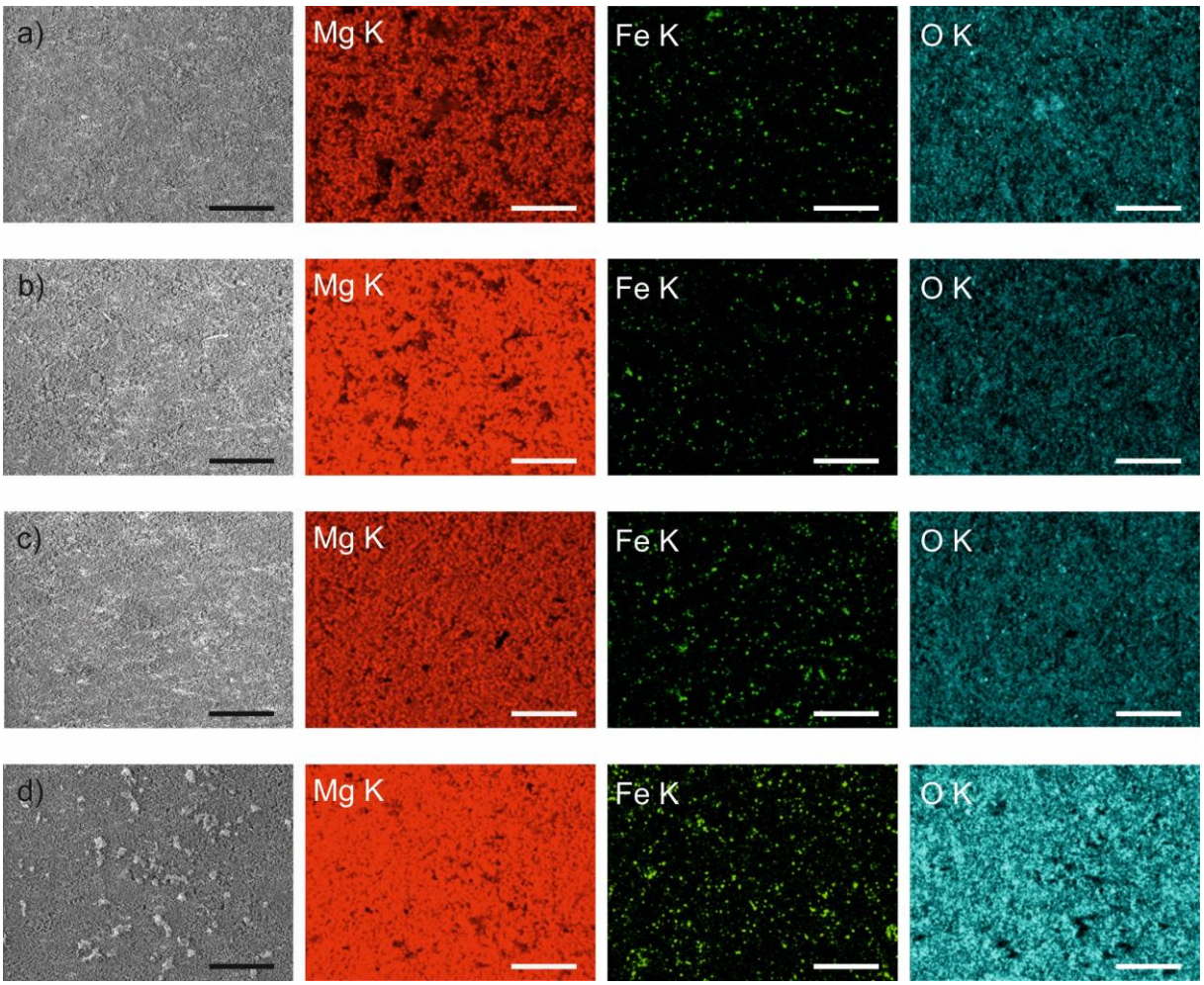

Fig. S22 SE-SEM micrographs and corresponding EDX images of the samples collected from different layers of the Mg-Fe system after cyclic separation experiments (15 kV): 1st (a), 2nd (b), 3rd (c), 4th (d). The sample numbers correspond to the number presented in Fig. 4a. Scale bars in all cases: 250 µm.

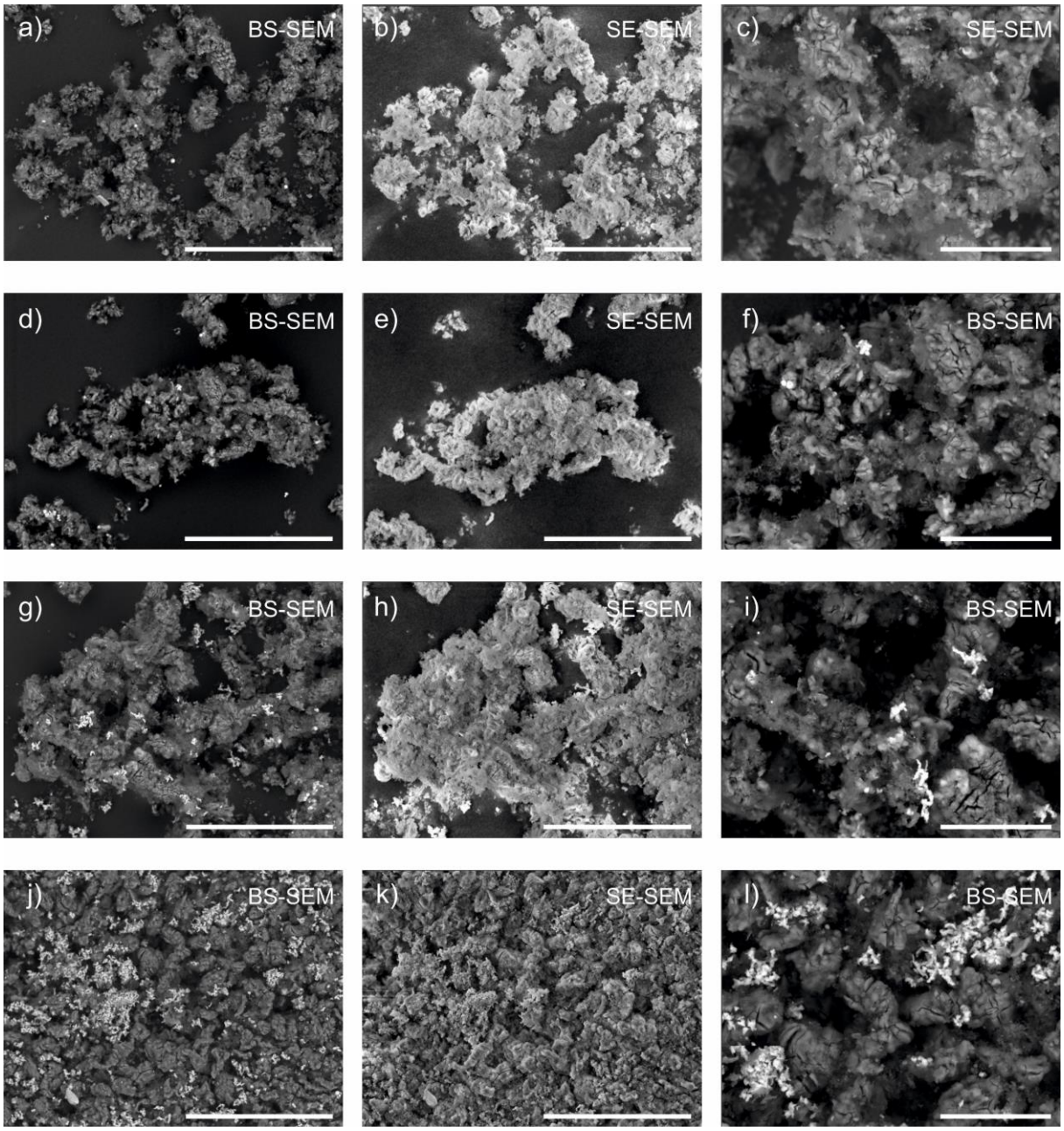

Fig. S23 SE-SEM and BS-SEM images obtained at different magnifications for the samples collected from the Mg-Fe system after cyclic separation experiments (15 kV): 1st (a,b,c), 2nd (d,e,f,), 3rd (g,h,i), 4th (j,k,l). The layers' sample numbers correspond to the number presented in Fig. 4a. Scale bars: 100 µm (a,b,d,e,g,h,j,i), 30 µm (c,f,i,l).

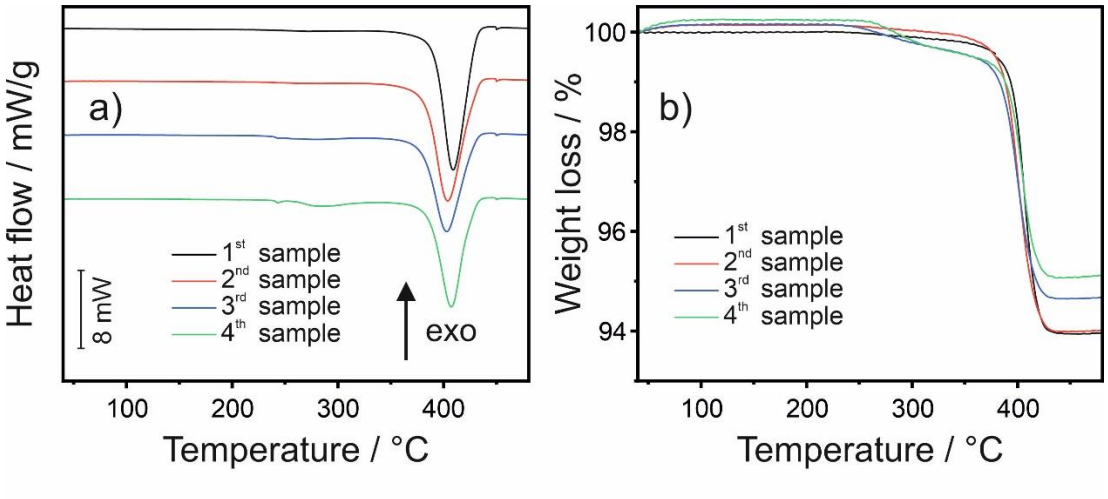

Fig. S24 DSC (a) and TG (b) curves obtained for the hydrogenated Mg-Fe system powder samples collected from different layers (the sample numbers correspond to the number presented in Fig. 4a) in the autoclave after a series of hydrogenation/dehydrogenation experiments run under 20 bar H_2, 100 bar of CH_4/H_2 gas mixture (20 bar of partial H_2 pressure), and 100 bar of natural gas/H_2 gas mixture (20 bar of partial H_2 pressure). The heating was performed at 10 °C/min. The heat flow has been normalized to the mass of the sample.

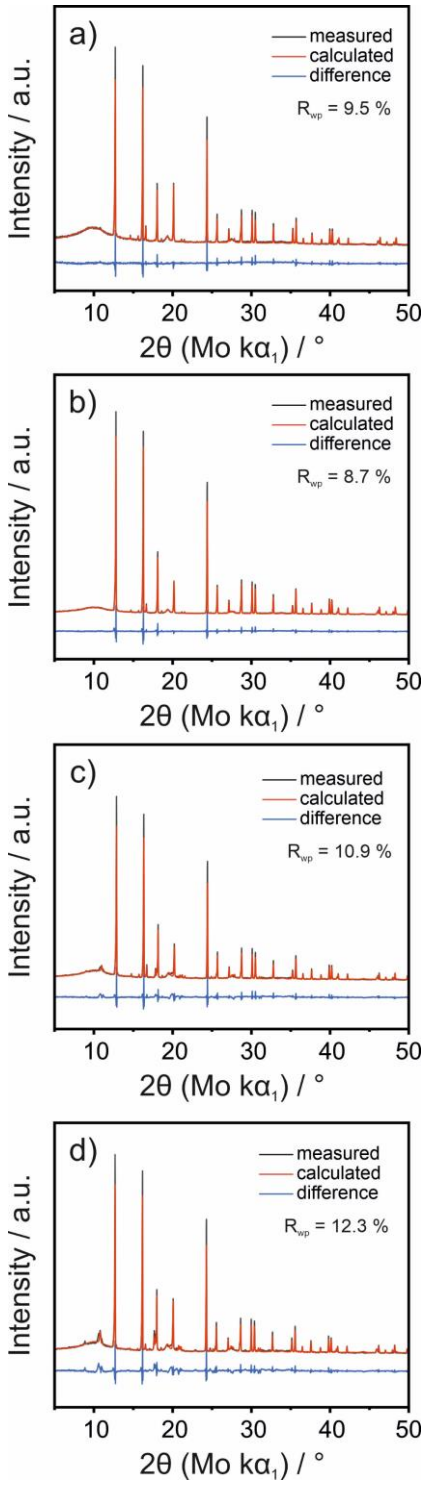

Fig. S25 XRD patterns and Rietveld refinement plots of the samples collected from different layers of the Mg-Fe system after cyclic separation experiments: 1st (a), 2nd (b), 3rd (c), 4th (d). The patterns were fitted using the following phases: Fe ICSD-48382 (ICSD release 2024.1), Mg ICSD-258531 (ICSD release 2024.1), Mg_2FeH_6 ICSD-107500 (ICSD release 2024.1), MgH_2 ICSD-155807 (ICSD release 2024.1), MgO ICSD-158103 (ICSD release 2024.1), Ni ICSD-8688 (ICSD release 2024.1). The sample numbers correspond to the number presented in Fig. 4a.

S8. Mg-Ni system after separation of H_2 from H_2/CO_2 gas mixtures

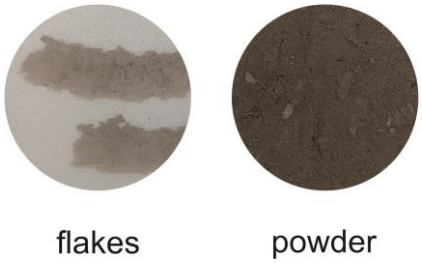

Fig. S26 Pictures of the flakes and powder of the Mg-Ni system material after four cycles of hydrogenation/dehydrogenation experiments under ~ 50 bar of H_2/CO_2 gas mixture (0.5 bar of partial CO_2 pressure). The sample names correspond to those presented in Fig. 5e.

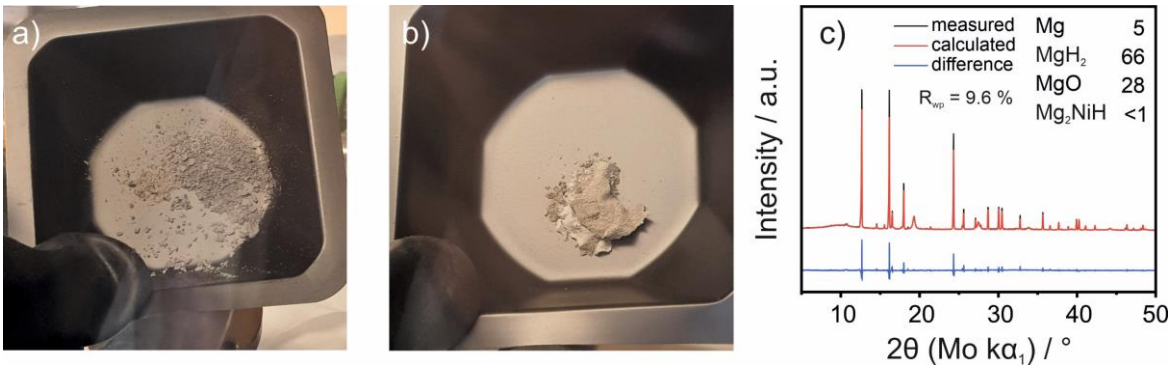

Fig. S27 (a,b) Photos of the Mg-Ni system material after four cycles of hydrogenation under ~ 50 bar of H_2/CO_2 gas mixture (0.5 bar of partial CO_2 pressure) in powder and flake form, respectively. The sample names correspond to those presented in Fig. 5e. The powdered sample partially covers the flakes; c) XRD pattern (and Rietveld refinement plot) of the hydrogenated Mg-Ni system flake sample. The concentrations of the main phases are presented in wt.%.

S9. Mg-Fe system after separation of H_2 from H_2/CO_2 gas mixtures

Fig. S28 Picture of the powder of the Mg-Fe system material after four cycles of hydrogenation/dehydrogenation experiments under ~ 50 bar of H_2/CO_2 gas mixture (0.5 bar of partial CO_2 pressure).

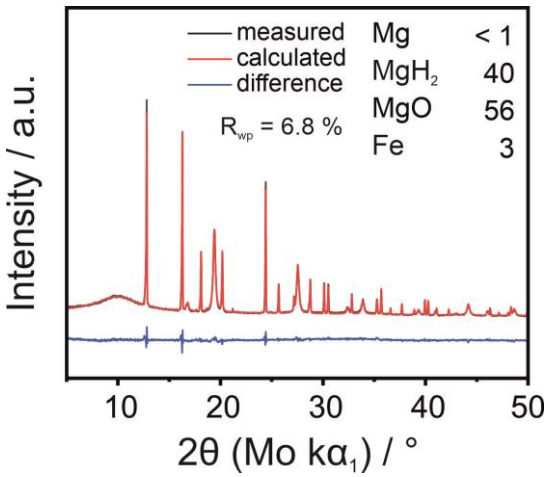

Fig. S29 XRD pattern (and Rietveld refinement plot) of the hydrogenated Mg-Fe system powder sample (after four cycles of hydrogenation/dehydrogenation experiments under ~ 50 bar of H_2/CO_2 gas mixture). The concentrations of the main phases are presented in wt.%

S10. Literature comparison of different H_2 separation techniques

Table S2 Comparison of different H_2 separation techniques.

Separation method	Gas mixture	H_2 conc. / vol. %	H_2 rcy / %	H_2 purity / %	Ref.
PSA	H_2:N_2:CH_4:Ar (58:25:15:2)	58	55.5-75.3	99.25-99.97	[S4]
Cryo-Cooling	H_2:CH_4:C_2H_6:C_3H_8:N_2:C_6H_6 (55:39:2:1:2:1)	55	25.1	88.1	[S5]
Membrane	H_2+NH_3	60	86	<99	[S6]
Membrane+PSA	H_2+CH_4	4	<60	99.97	[S7]
Electrochemical pump	H_2+CH_4	5	87	<300 ppm CH_4	[S8]
	H_2+CH_4	5	91.72	<99.1	[S9]
Metal hydride:					
$LaNi_{4.8}Mn_{0.3}Fe_{0.1}$	H_2+CH_4	10	74	>99	[S10]
MgH_2	H_2+CH_4	10	~99.9		[S3]
	H_2+CH_4	20		>99.9	This work

H_2 conc. – hydrogen concentration

H_2 rcy – hydrogen recovery

PSA – Pressure Swing Absortpion technique

Table S2 shows a general comparison of H_2 separation techniques. Some of the methods, like adsorption techniques (e.g. PSA- Pressure Swing Adsorption) are chosen, when high H_2 contents in the gas mixture are awaited. The adsorbents used in this case are usually active in absorbing all components of the gas mixture except H_2. H_2 is rather flowing through the adsorption columns. In the metal hydride reactors (like in the case of Mg-based systems), H_2 is the gas, to be captured by the used adsorbents (metals). The H_2-rich gas mixtures, as being used with PSA, would not be economically to be separated by metal hydride reactors because of increased volume and adsorbents demand. Nevertheless, the metal hydride-based separation systems performance could be compared with electrochemical hydrogen pumps. Both technologies show satisfactory H_2 recovery and purity. However, it should be emphasized that Table S2 present mainly data obtained under different laboratory conditions (e.g. batch reaction in case of MgH_2-based separation and experiments using adapted fuel cell test stand in the case of electrochemical pumps). Therefore, the proper benchmarking of different technologies requires detailed analysis of separation techniques on the system level. In this case, it includes not only additional hydrogen separation parameters (like amount of hydrogen separated in time) but also the economic aspects including for example material costs and necessary energy operation input.

References

S1. https://fnb-gas.de/en/hydrogen-core-network/. [Online] Homepage of german Vereinigung der Fernleitungsnetzbetreiber Gas e.V. (FNB Gas), 14 March 2024.

S2. https://www.vgbe.energy/en/news/vgbe-factsheet-h2-readiness-for-gas-turbine-plants-published/. [Online] Homepage of German vgbe energy e.V. factsheet "H_2 readiness for gas turbine plants", 2023

S3. A. Woeste, M. Balcerzak, R. Urbanczyk, M. Felderhoff, *Energy Technol.*, 2021, 9, 2001079. https://doi.org/10.1002/ente.202001079

S4. M. Yáñez, F. Relvas, A. Ortiz, D. Gorri, A. Mendes, I. Ortiz, PSA purification of waste hydrogen from ammonia plants to fuel cell grade, *Sep. Purif. Technol.,* 2020, 240, 116334. https://doi.org/10.1016/j.seppur.2019.116334.

S5. M. Aasadnia, M. Mehrpooya, B. Ghorbani, A novel integrated structure for hydrogen purification using the cryogenic method, *J. Cleaner Prod.*, 2012, 278, 123872. https://doi.org/10.1016/j.jclepro.2020.123872.

S6. D. Werner, Gasreinigungsverfahren für große Wasserstoff-Mengen. *Chem. Ing. Tech.*, 1981, 53, 73-81. https://doi.org/10.1002/cite.330530202.

S7. W. Liemberger, M. Groß, M. Miltner, M. Harasek, Experimental analysis of membrane and pressure swing adsorption (PSA) for the hydrogen separation from natural gas, *J. Cleaner Prod.*, 2017, 167, 896-907. https://doi.org/10.1016/j.jclepro.2017.08.012.

S8. S. Mrusek, M. Blasius, F. Morgenroth, S. Thiele, P. Wasserscheid, Hydrogen extraction from methane-hydrogen mixtures from the natural gas grid by means of electrochemical hydrogen separation and compression, *Int. J. Hydrogen Energy*, 2024, 50(A), 526-538. https://doi.org/10.1016/j.ijhydene.2023.08.195

S9. K. Arunagiri, J.M. Turssline, C.G. Arges, Purifying Hydrogen from Dilute Hydrogen–Natural Gas Mixtures Using HT-PEM Electrochemical Hydrogen Pumps, *ACS Energy Lett*. 2024, 9, 2912-2919. https://doi.org/10.1021/acsenergylett.4c00746

S10. D. Dunikov, D. Blinov, Extraction of hydrogen from a lean mixture with methane by metal hydride, *Int. J. Hydrogen Energy*, 2020, 45, 9914-9926, https://doi.org/10.1016/j.ijhydene.2020.01.201